Incorporation of Eu^{3+} in $ZnGa_2O_4:Ni^{2+}$ for improved NIR persistent luminescence located in second transparency window

Minghui Jin[1], Tao Zhang[2], Ji-Guang Li[3], Qi Zhu[1*]

[1]*Key Laboratory for Anisotropy and Texture of Materials (Ministry of Education), School of Materials Science and Engineering, Northeastern University, Shenyang, Liaoning 110819, PR China*

[2]*Shenyang National Laboratory for Materials Science, Northeastern University, 3-11 Wenhua Road, Shenyang 110819, China*

[3]*Research Center for Functional Materials, National Institute for Materials Science, Namiki 1-1, Tsukuba, Ibaraki 305-0044, Japan*

*Corresponding author

Dr. Qi Zhu

Tel: +86-24-8367-2700

E-mail: zhuq@smm.neu.edu.cn

Abstract

It is well known that near-infrared (NIR) persistent phosphors have rather low absorption coefficients of biological tissues for NIR light. However, recent research shows that the phosphors emitting NIR lights in second (NIR-II, 1000-1350 nm) and third (NIR-III, 1500-1800 nm) biological window have advantages over that in NIR-I (650-900 nm). Although $ZnGa_2O_4:Ni^{2+}$ outputs near-infrared (NIR) emission and afterglow located in NIR-II, the weak signal significant limits its application. Here, persistent luminescent phosphors of $ZnGa_2O_4:xNi^{2+}$, yEu^{3+} ($x = 0\text{-}0.013$, $y = 0.01\text{-}0.06$) (termed as ZEGN) were synthesized via a traditional high-temperature solid-state reaction, which feature a broad emission band in the second near-infrared (NIR-II) window. Upon ultraviolet (UV) or orange-red lights excitation, the phosphors exhibit a broad NIR emission at about 1300 nm, arising from the $^3T_2(^3F)\rightarrow{}^3A_2(^3F)$ transition of Ni^{2+}. However, incorporation of Eu^{3+} ions, the NIR emission intensity significantly increases with the increase of Ni^{2+} ion concentration, reaching the maximum by 18 times at $x = 0.005$. Removing the light source yields intense NIR afterglow and red afterglow, with the duration longer than 500 s. It is worth noting that the red afterglow of Eu^{3+} shows a dramatically decrease but the NIR afterglow increases with increasing the Ni^{2+} ion concentration, because of energy transfer. Under the excitation of 282-nm UV light, the ZGEN sample exhibits a good thermal stability. The phosphor offers a promising application in biological imaging due to broadband NIR-II light and afterglow.

Keywords: $ZnGa_2O_4$; Ni^{2+}; near-infrared (NIR); second transparency window; persistent phosphors

1. Introduction

Fluorescence imaging is widely used in fields such as life sciences and clinical medicine due to its advantages of non-invasive, high sensitivity, and high spatiotemporal resolution.[1-3] Indeed, near-infrared (NIR) light can penetrate biological tissues, such as skin and blood, more efficiently than visible light, while the light in the second NIR window (1000-1400 nm) has lower absorption, lower scattering and more efficient tissue penetration than the light in the first NIR window (650-950 nm).[4] Therefore, the optical signal in the second window range of near-infrared can greatly improve the penetration depth, resolution, and signal-to-noise ratio of live imaging.[1, 5] Traditional fluorescence imaging requires the use of external excitation light sources to excite real-time fluorescent probes inside the organism, inevitably resulting in the generation of biological tissue background fluorescence, which affects the resolution and signal-to-noise ratio of imaging.[6] Long afterglow is a unique optical phenomenon that refers to the slow release of stored light energy by a material after stopping excitation (usually ultraviolet, X-ray, etc.), lasting for several minutes, hours, or even days. [7-9] Generally speaking, unlike traditional fluorescence imaging, long afterglow imaging does not require real-time excitation from external light sources, thus effectively avoiding interference from spontaneous fluorescence of biological tissues caused by excitation, thereby improving the resolution of in vivo imaging.

Transition metal ions, as the candidate dopants to realize a broadband NIR luminescence, have attracted considerable attention.[10] Among them, Ni^{2+} ions give a broadband NIR emission with a center around ~ 1300 nm when occupying an octahedral site in various materials, such as Ni^{2+}-doped $ZnAl_2O_4$ nanostructures,[11, 12] Ni^{2+}-doped β-Ga_2O_3 nanocrystals,[13] Ni^{2+}-doped yttrium aluminum gallium garnet phosphors[14] and so on, which is attributed to both its $3d^8$ electronic configuration and strong influence on the splitting of the energy level caused by the electrostatic potential, owing to the contribution of neighborhood ions. Researchers have made many attempts to improve the emission intensity of this fluorescent powder, such as increasing the excess or deficiency of Zn^{2+} in the raw material,[15] doping Ge^{4+}, Mg^{2+}, or Li^+ with average charge,[16, 17] and adjusting the crystal field by doping Al^{3+}, Sn^{4+} or other elements to change the proportion of ions in the matrix.[6, 14, 18] All of the above methods essentially adjust the matrix lattice, that is, the direct environment in which the activated ions are located, thereby achieving an increase in material emission intensity, but rarely involving in energy transfer. As a rule of thumb, if the emission spectrum of the donor ions overlaps with the excitation spectrum of the acceptor ions, energy transfer usually occurs, which could increase the emission intensity of the phosphor.[19-21] Eu^{3+} ion, which shows an intense emission at about 616 nm ($^5D_0 \rightarrow {}^7F_2$ transition), is the activator of red fluorescent powder for color television. It is interesting to note that the NIR absorption of octahedral Ni^{2+} and emission of Eu^{3+} partially overlap in spectra.[18, 19, 21] Therefore, energy transfer from Eu^{3+} to Ni^{2+} in Eu^{3+}/Ni^{2+} co-doped $ZnGa_2O_4$ may occur, making the emission intensity of Ni^{2+} increase.

Herein, a series of $ZnGa_2O_4:Ni^{2+}, Eu^{3+}$ NIR phosphors were successfully synthesized using a solid-state reaction. Under the excitation of ultraviolet light, the energy transfer from Eu^{3+} to Ni^{2+} results in a significant increase by 18 times in the near-infrared emission and afterglow of Ni^{2+} ions, indicating that the phosphors are potential fluorescent materials for biological imaging field.

2. Experimental Section

2.1. Materials and synthesis

$ZnGa_2O_4:yEu^{3+}$ (y = 0.01, 0.02, 0.04, 0.06) and $ZnGa_2O_4:xNi^{2+},0.02Eu^{3+}$, ($x$ = 0, 0.003, 0.005, 0.008, 0.01, 0.013) (called as ZGE and ZGEN in the following content) phosphor powders were prepared by a conventional high-temperature solid-state reaction. The raw materials (ZnO, Ga_2O_3, Eu_2O_3, and NiO) were all purchased from Sinopharm (Shanghai, China) with a high purity of 99.9%. All the materials were calculated accurately and were ground for 30 minutes to be fully mixed at the beginning. Then, the powder mixture was pre-sintered at 1000 ℃ for 4 hours under air conditions and ground for 30 min again, they were finally sintered at 1350 ℃ in air atmosphere for 8 h. The samples were slowly cooled to room temperature and grinded again about 30 min for the later test.

2.2. Characterization.

Phase identification was performed via X-ray diffractometry (XRD, Bragg measurement, SmartLab, Rigaku, Tokyo, Japan) under 40 kV/200 mA using nickel-filtered Cu-Kα radiation and a scanning speed of 10° 2θ per minute from 10° to 70°. Product morphology and microstructure were analyzed by transmission electron microscopy (TEM, Model JEM-2000FX, JEOL) under 200 kV. Photoluminescence of Eu^{3+} was analyzed with an FP-8600 fluorospectrophotometer (JASCO, Tokyo) equipped with a Φ60 mm integrating sphere (Model ISF-834, JASCO), a 150 W xenon lamp for excitation, a slit width of 5 nm and a scan speed of 100 nm/min for both excitation and emission. The spectral response of the spectrophotometer was corrected with a Rhodamine-B solution ($5.5\ g \cdot L^{-1}$ in ethylene glycol) and a standard light source unit (ECS-333, JASCO) for the ranges of 220-600 nm and 350-850 nm, respectively. The fluorescence decay of Eu^{3+} was also analyzed with the FP-8600 instrument and long-last persistent luminescence decay curves of Eu^{3+} was recorded by using a Horiba JY Fluorolog-3 (Kyoto, Japan) spectrofluorometer equipped with 150 W xenon lamps at room temperature. Meanwhile, Horiba JY Fluorolog-3 (Kyoto, Japan) was used to detect the photoluminescence spectrum (PL)/photoluminescence excitation spectrum (PLE) and long-last persistent luminescence decay curves of Ni^{2+}. Before persistent luminescence tests, the samples were excited by a 365-nm UV lamp for 5 min.

3. Results and discussion

3.1 Phase identification and crystal structure

$ZnGa_2O_4$, an oxide compound with a spinel structure, belongs to the cubic crystal system with the formula AB_2O_4, in which the oxygen ions are densely packed in a face-centered cubic configuration with Zn^{2+} ions in the A site (tetrahedral site) and Ga^{3+} ions in the B site (octahedral site).[22] According to the relevant literature,[23] Eu^{3+} and Ni^{2+} should occupy the octahedral coordination of Ga^{3+}, because Ni^{2+} and Eu^{3+} for ions have the same valence state and similar ionic radii and Ga^{3+} ions, respectively. Figure.1a shows a schematic diagram of the crystal structure with the ions occupying tendency

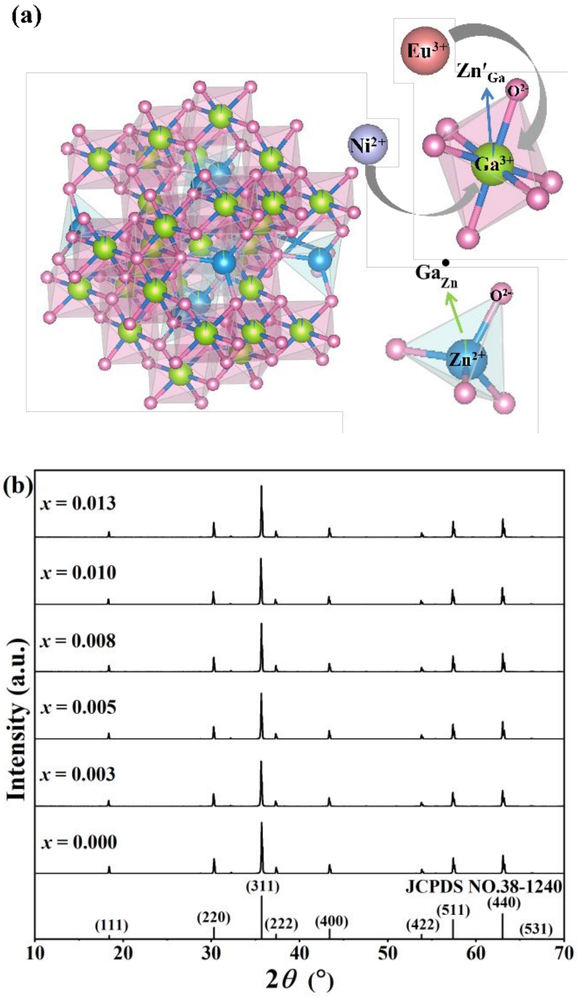

FIGURE 1 (a) Crystal structure and (b) XRD patterns of ZGEN sample

for better understand. The XRD patterns of ZGE and ZGEN synthesized by the traditional high-temperature solid-state reaction were shown in Figure S1 and Figure 1b (we get the best content of Eu^{3+} from the following experiments, $y = 0.02$). It can be seen that all of the samples' diffraction peaks are well matched to the standard diffraction of $ZnGa_2O_4$ (JCPDS No. 38-1240), indicating that the prepared samples are a single phase.

Figure 2a and d show the TEM morphology of the typical sample of ZGEN (x = 0.005). It can be indicated that they are irregularly shaped particles of approximately 250 nm in size. Selected area electron diffraction (SAED) and high-resolution transmission electron microscopy (HR-TEM) were performed for the single particle, as shown in Figure 2b and c. The high crystallinity of the sample is confirmed by the clear lattice stripes in the HR-TEM image. The distances between the two crystal planes with different orientations are respectively measured to be ~ 0.296 and 0.253 nm with an angle of about 58.5°, so they are corresponding to the (220) and (311) crystallographic planes, matching well with the d (220) = 0.295 nm and the d (311) = 0.253 nm of the cubic structured $ZnGa_2O_4$ (JCPDS No. 38-1240). The SAED pattern shows symmetric lattice-grid characteristics, indicating the sample is single crystal. The elemental distribution results in Figure 2e-i show the successful doping of Ni and Eu and the homogeneous distribution of the chemical elements.

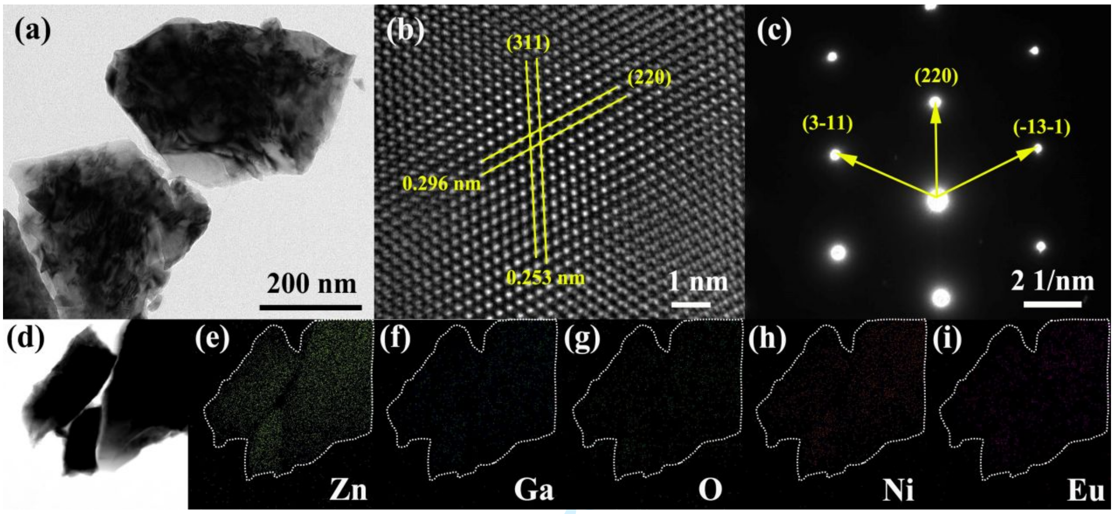

FIGURE 2 (a and d) TEM image, (b) HR-TEM image, (c) SAED pattern, (e-i) elemental mapping of the $x = 0.005$ sample. (e-i) Element distributions of (e) Zn, (f) Ga, (g) O, (h) Ni, and (i) Eu, respectively

3.2. Photoluminescence of the ZGE phosphors

PLE and PL spectra of ZGE phosphors ($x = 0$) were shown in Figure 3. Monitored at 616 nm, a strong band was found from 250 nm to 350 nm centered at ~ 282 nm, which can be attributed to the O^{2-}-Eu^{3+} charge transfer. According to the reports,[24, 25] the other bands centered at 361, 392 and 464 nm corresponding to the transitions $^7F_0 \rightarrow {}^5D_4$, $^7F_0 \rightarrow {}^5L_6$ and $^7F_0 \rightarrow {}^5D_2$ of Eu^{3+} ions respectively. Under excitation with 282 nm UV light, the ZGE phosphors show sharp lines from 550 nm to 750 nm, which are related to the typical transition of Eu^{3+} from the excited $^5D_0$ to the ^7F_J ($J = 0, 1, 2, 3, 4$) emission states with the $^5D_0 \rightarrow {}^7F_2$ red one being the most prominent.[25, 26] In addition, as shown in the inset of Figure 3, the emission intensity gradually increases with increasing the content of Eu^{3+}. After the intensity reaching a maximum value when y = 0.02, it gradually decreases with further increasing the concentration of Eu^{3+} due to the concentration quenching effect.

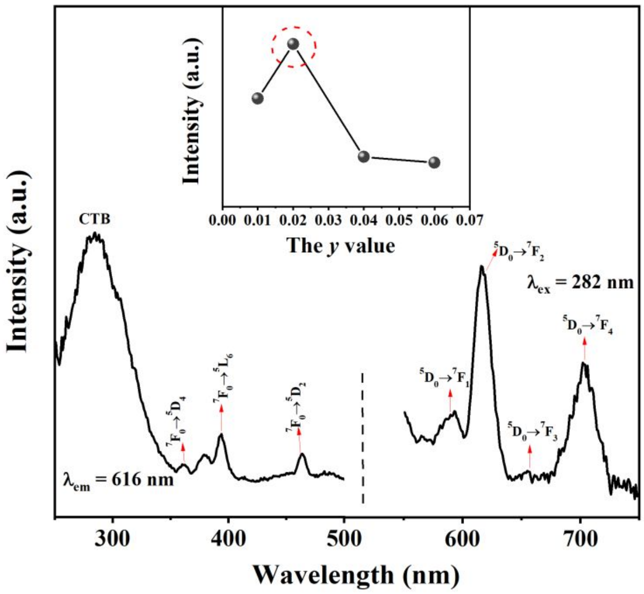

FIGURE 3 PLE and PL spectra of ZGE samples

3.3. Photoluminescence and energy transfer of the ZGEN phosphors

Figure 4a shows the PL spectrum of the $ZnGa_2O_4$:0.02Eu^{3+} phosphor under excitation at 282 nm and the PLE spectrum of the $ZnGa_2O_4$:0.005Ni^{2+} phosphor monitored at 1310 nm. It can be seen that the emission spectrum of $ZnGa_2O_4$:0.02Eu^{3+} and the excitation spectrum of $ZnGa_2O_4$:0.005Ni^{2+} have a large overlap in the wavelength range from 570 nm to 630 nm. Theoretically, if the emission spectrum of the donor ion overlaps with the excitation spectrum of the recipient ion, energy transfer usually occurs between them. So maybe, there will be energy transfer between Ni^{2+} and Eu^{3+} in $ZnGa_2O_4$ system. Energy level diagram between Ni^{2+} and Eu^{3+} was shown in Figure 4b, it can be seen that some of the energy levels of the two ions are adjacent, therefore, there is a high possibility of energy transfer from Eu^{3+} to Ni^{2+} during the emission process. Based on the previous investigations, the electron transitions and energy transfer process of the samples may be as following. Under ultraviolet excitation, the electrons in the Ni^{2+} ion are excited from the ground state to the excited state energy level, then relax to the lowest excited state $^3T_2$ and then returned to the ground state

$^3A_2$, producing NIR emission at 1310 nm.[27] In addition, the electrons in Eu^{3+} ions are excited from the ground state $^7F_0$ to the excited states ^5D_J (J=1,2,3.4) and then part of the electrons relax to the lowest excited state $^5D_0$, and then return to the ground state in the form of radiative transitions, resulting in a red emission of 616 nm.[25, 26] Meanwhile, part of the electron energy at the excited state level $^5D_0$ is transferred to the excited state level $^3T_1(^3F)$ of adjacent Ni^{2+} ions, making the NIR emission of Ni^{2+} improve.

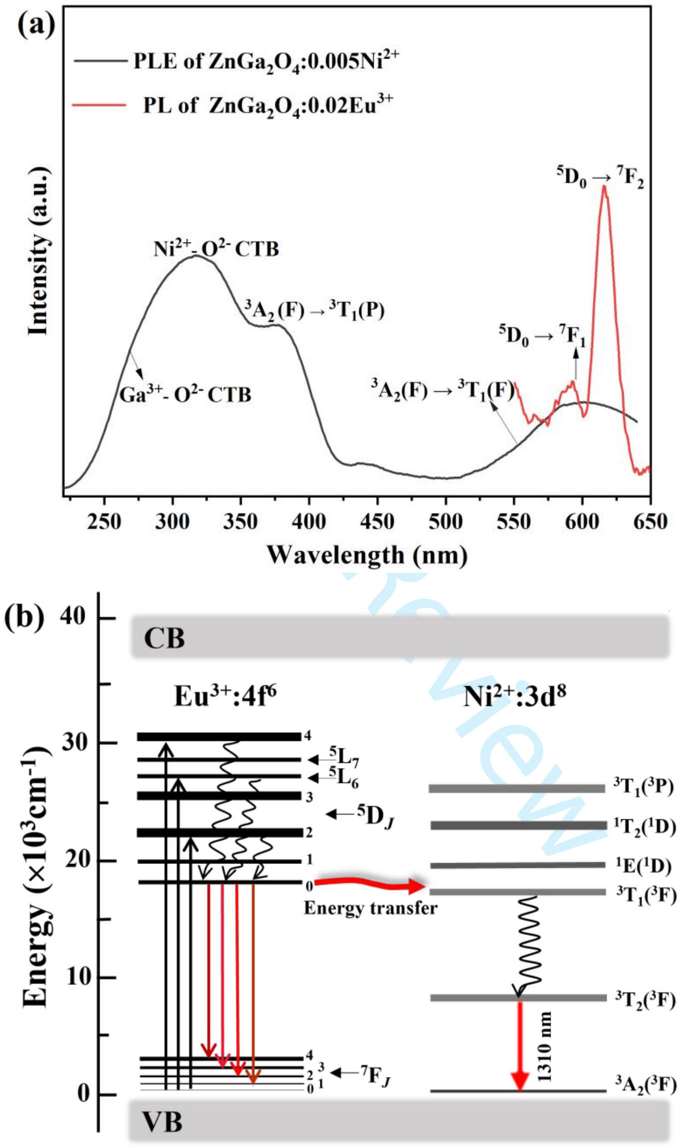

FIGURE 4 (a) PLE spectra of $ZnGa_2O_4$:0.005Ni^{2+} and PL spectra of $ZnGa_2O_4$:0.02Eu^{3+} and (b) Schematic illustration for the energy transfer process between Ni^{2+} and Eu^{3+} in ZGEN phosphors, with the energy level location referring to the literatures

To determine whether this energy transfer exists in the system, we synthesized a series of ZGEN (x = 0-0.013) phosphors doping both Ni^{2+} and Eu^{3+} ions (the optimal doping amount of Eu^{3+} is y = 0.02). Figure 5 shows the PLE spectrum of ZGEN phosphors monitored at 1310 nm, which are consistent with a typical fluorescence pattern of $ZnGa_2O_4$ doped with Ni^{2+}. The first excitation band centered at 250 ~ 350 should be generated by a combination of overlapping bands: the Ga^{3+} - O^{2-} charge transfer band (CTB) at ~ 244 nm,[28] Eu^{3+}-O^{2-} CTB of at ~ 282 nm [26] and the Ni^{2+}-O^{2-} CTB at ~ 310 nm.[27] In addition, the bands centered at ~ 378 and ~ 610 nm respectively correspond to the 3d-3d transition of ${}^3A_2(F)\rightarrow{}^3T_1(P)$ and ${}^3A_2(F)\rightarrow{}^3T_1(F)$ of the Ni^{2+} ion [29]. The PL spectra of ZGEN phosphors at 282 nm excitation spectrum are shown in Figure 5b. The PL spectrum shows a same broadband emission caused by the ${}^3T_2(F)\rightarrow{}^3A_2(F)$ transition of Ni^{2+}. It can also be seen that, the emission intensity increases gradually with increasing Ni^{2+} content, and the intensity reaches a maximum value at a Ni^{2+} concentration of 0.5 mol%, then, the intensity gradually decreases with furthering increasing the Ni^{2+} content, which is due to the concentration quenching effect. With the increase of nickel ion content, however, the intensity of Eu^{3+} dramatically decreases. The variations of Ni^{2+} and Eu^{3+} emissions are similar to the typical variation pattern presented in other sensitizer-activator systems,[10, 20] based on this feature, it can be inferred that there is a phenomenon of energy transfer between Ni^{2+} and Eu^{3+}.

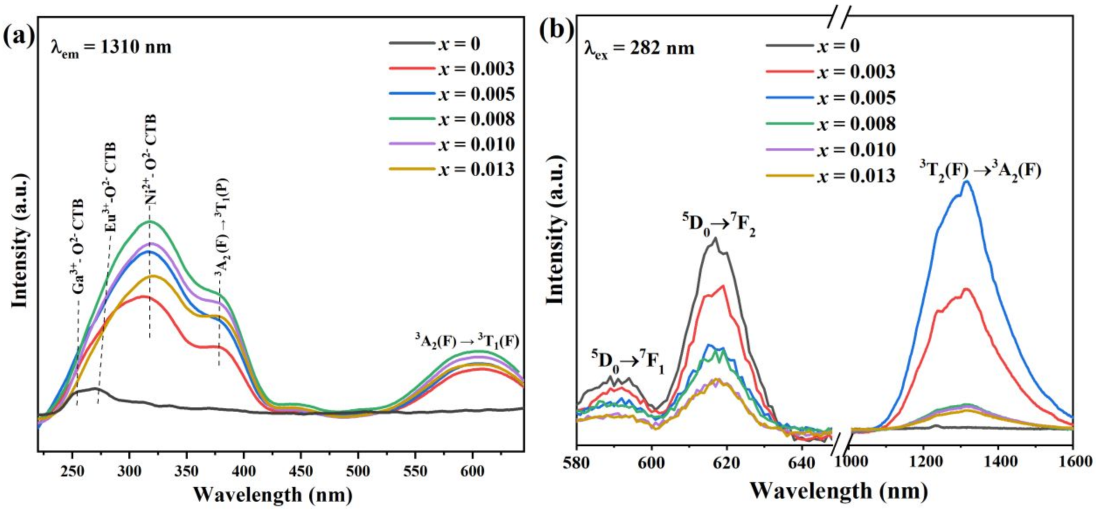

FIGURE 5 (a) PLE and (b) PL spectra of ZGEN samples

The energy transfer efficiency can be calculated by the following equation:[20, 30]

$$\eta_{\tau} = 1 - I_s/I_{s0} \tag{1}$$

where, I_s represents the integral intensity of the emission spectrum of Eu^{3+} in the presence of Ni^{2+}, I_{s0} represents the integral intensity of the emission spectrum of Eu^{3+} in the absence of Ni^{2+}, η_{τ} is the energy transfer efficiency. Figure 6a-c shows fluorescence decay curves of ZGEN samples (x = 0, 0.003 and 0.005) and based on the calculation above, energy transfer efficiencies of 21.77% and 45.51% were determined for x = 0.003 and 0.005, respectively. R_c (the critical distance) is the key parameter for assessing the average distance between activator and activator or sensitizer and activator when a concentration quenching effect plays a role and it can be calculated by the following equation:[31]

$$R_c = 2\left[\frac{3V}{4\pi x_c N}\right]^{\frac{1}{3}} \tag{2}$$

where, x_c is the critical concentration of Ni^{2+} ions, V is the volume of the unit cell and N represents the number of positions per unit cell available for the dopant (Ni^{2+}). In this study, the values for V, x_c and N are 578.01 Å^3, 0.005 and 16, respectively. Based on these values, R_c of 30.21 Å was calculated.

The exchange interaction and the electric multipolar interaction are the two models which can be used to understood the concentration quenching effect.[20] In this work, the concentration quenching effect should be excluded from the exchange interaction model, because the value of R_c (30.21 Å) is much larger than 5 Å.[32] According to Dexter's theory, the type of work for electric multipolar interaction can be estimated by the following equation:[20, 33]

$$\frac{\eta_o}{\eta} \propto C^{\frac{n}{3}} \tag{3}$$

Here, η_0/η represents the ratio of the initial luminescence quantum efficiency of Eu^{3+} to the luminescence quantum efficiency of Eu^{3+} in the Ni^{2+} doped phosphor, which can be approximated by the ratio of the initial luminescence intensity of Eu^{3+} to the luminescence intensity of Eu^{3+} in the Ni^{2+} doped phosphor instead. Values of 6, 8 and 10 for n represent dipole-dipole (d-d), dipole-quadrupole (d-p) and quadrupole-quadrupole (q-q) interactions respectively. Figure 6e-g represent I_{S0}/I_S as a function of

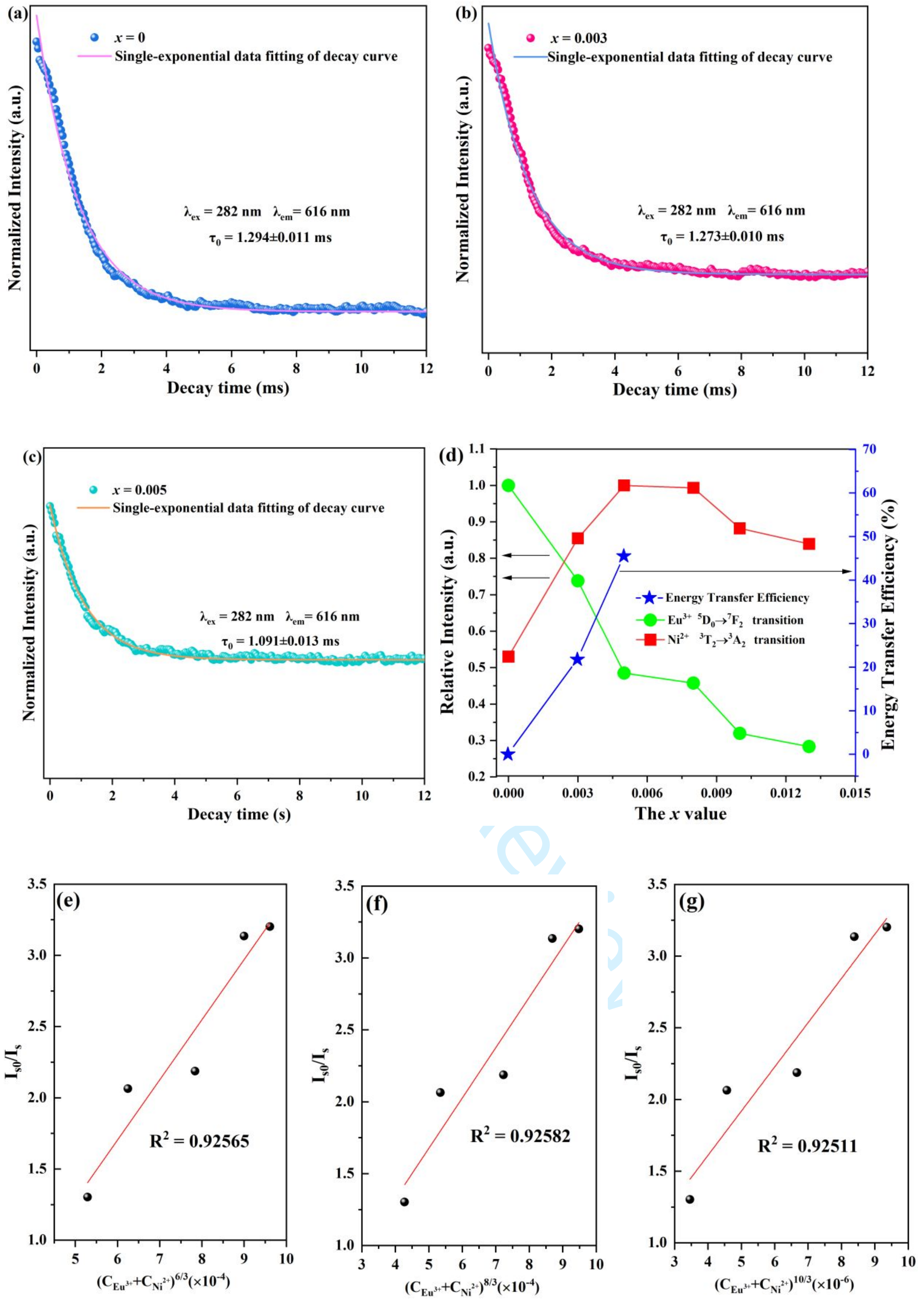

FIGURE 6 (a-c) Fluorescence decay curve and fitting results for the 616 nm emission of ZGEN ($x = 0, 0.003, 0.005$) and (d) Relative emission intensities of Ni^{2+} and Eu^{3+} at 282 nm and energy transfer efficiencies as functions of Ni^{2+}-doping concentrations (x). Relationships between I_{S0}/I_S and $C^{n/3}$ with (e) $n = 6$, (f) $n = 8$ and (g) $n = 10$

$C^{n/3}$ (n = 6, 8, 10). Based on a linear fit for each case, the correlation coefficient (R^2) is found to be a maximum of 0.92582 for n equals to 8. Therefore, the concentration burst effect in ZGEN phosphors is dominated by the d-p interaction mechanism.

The decay time reflects the luminescence dynamics of the energy transfer process.[20, 26] Monitored at 616 nm and 1310 nm, Eu^{3+} and Ni^{2+} ions respectively exhibit red afterglow and long near-infrared afterglow (Figure 7). After cessation of the UV excitation, the two persistent luminescence signals of the phosphors last at least 500 s. When $x = 0$, the intensity of the red afterglow is the maximum one. However, as the concentration of Ni^{2+} increases, the red afterglow sharply decreases, and the signal almost disappears when $x = 0.013$. This further illustrates the existence of energy transfer from Eu^{3+} ions to Ni^{2+} ions in this system. The near-infrared afterglow becomes more intense at higher Ni^{2+} content, reaching the maximum at $x = 0.005$, which also corresponds to the above spectral test results. The persistent luminescence mechanism in this work can be summarized in Figure 8b.

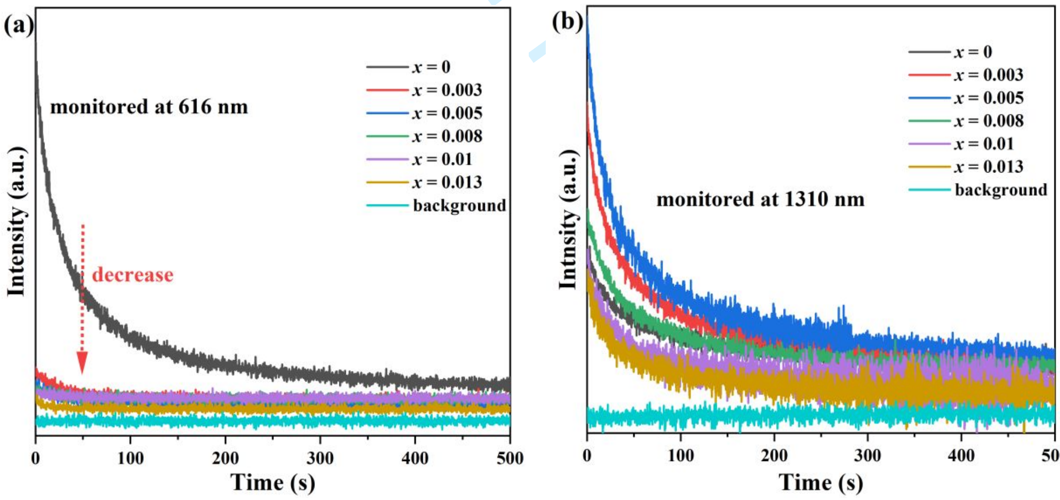

FIGURE 7 Persistent luminescence decay curves of ZGEN samples after 302 nm UV irradiation for 5 min

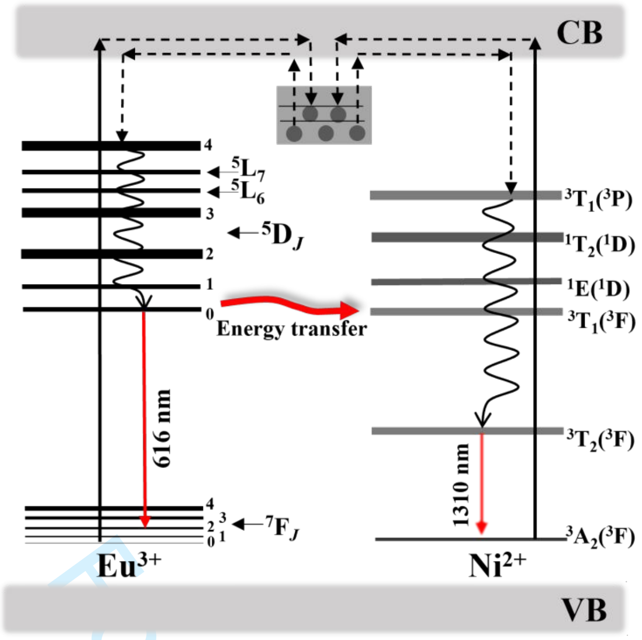

FIIGURE 8 A schematic representation of the possible persistent red and NIR luminescence mechanism in this work

Under the excitation of UV lamp (302 nm), the ground-state electrons of Eu^{3+} and Ni^{2+} ions are promoted to conduction band. The excited electrons are subsequently captured by the electron traps near the conduction band, which are filled during a sufficient illumination time. After the stopping the UV irradiation, recombination between the conduction electrons released from the electron traps and the excited energy levels of Eu^{3+} and Ni^{2+} finally contributes to both the NIR and red afterglows. However, electrons falling back to the excited energy level of Eu^{3+} ($^5D_0$) were partly transferred to excited energy level of Ni^{2+} ($^3T_1$), resulting in a significant decrease of red afterglow and an enhancement of near-infrared afterglow. The near-infrared afterglow intensity of x = 0.005 sample is 1.25 times that of x = 0 at the beginning of the decay time.

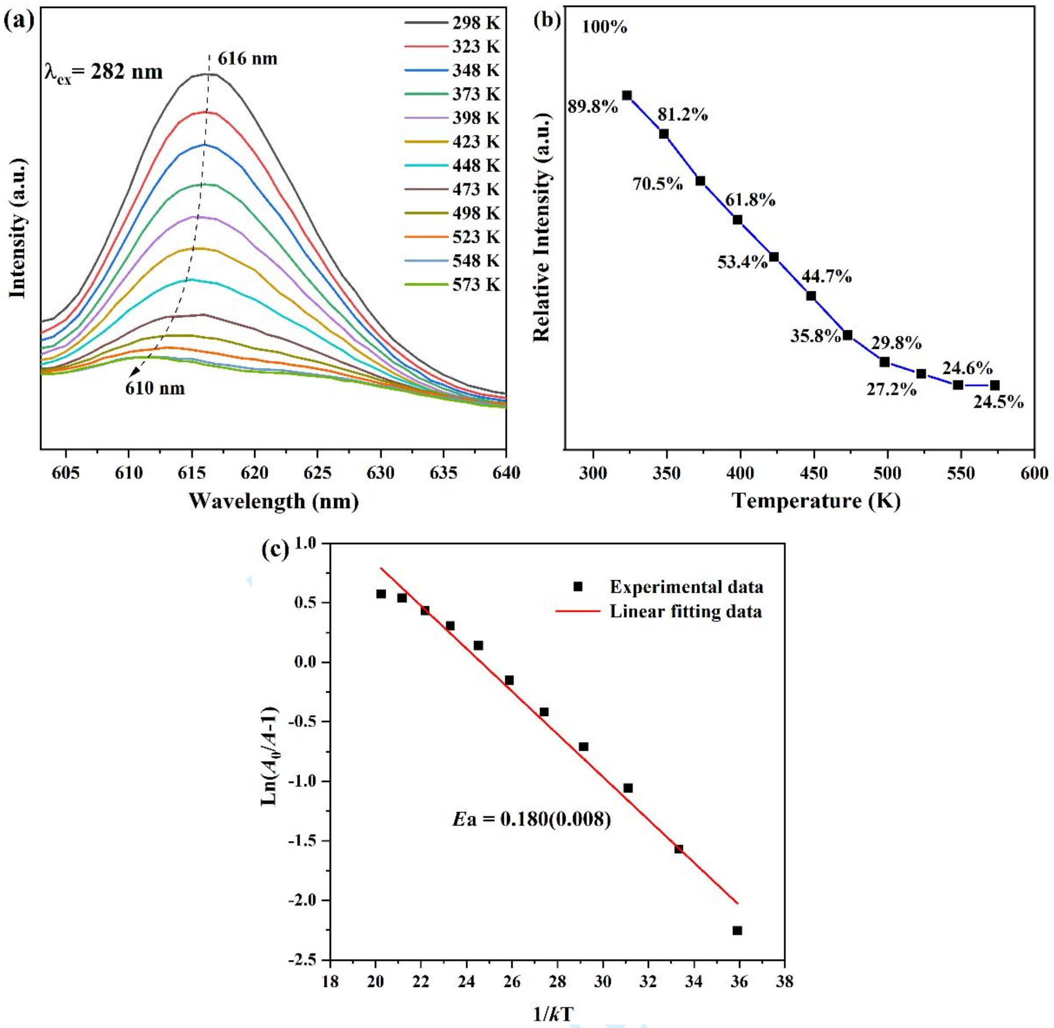

FIGURE 9 (a) Temperature-dependent luminescence spectra excited at 282 nm, (b) relative integral intensity of 616 nm emission bands, and (c) activation energy of thermal quenching for 616-nm emission bands at the temperature from 298 K to 573 K of ZEGN samples

Thermal quenching is one of the most important factors affecting the effectiveness of fluorescent powder. As shown in Figure 9a, the temperature-dependent luminescence spectra of the sample located in the red-light region (x = 0.005) were measured at the range of 298 K ~ 573 K under 282-nm UV excitation. Due to the thermal quenching behavior, however, it can be seen that the luminescence intensity of the fluorescent powder decreases with the temperature increasing. The decrease of luminescence intensity with the increase of temperature is due to the enhancement of molecular thermal motion at high temperature, which intensifies the nonradiative transition. In addition, a small blue shift of the emission peak from 616 nm to 610 nm was found by increasing the temperature, mainly due to the stokes displacement. When the temperature increases gradually, the molecular thermal motion increases gradually, and the crystal field intensity decreases, resulting in a lattice shrinkage distortion and the decrease of Stokes displacement.[34, 35] Taking the integral area of the emission peak as the object of intensity comparison and the emission peak intensity of 298 K as the benchmark, we calculated the intensity ratio of the integral intensity compared with the benchmark at different temperatures. Figure 9b shows its relative integrated emission intensity curves and the luminous intensity of the sample still reaches 70.50% even if the temperature rises to 100 °C. Figure 9c exhibits the $\ln(A_0/A-1)$ versus $1/kT$ plot for the emission of Eu^{3+}, from which the value of thermal activation energy (Ea) was determined to be ~ 0.180 eV by the following formula:

$$A=\frac{A_0}{1+c\,exp\,(-\frac{Ea}{kT})} \tag{4}$$

where A_0 and A are the integral area of the emission peaks at room temperature (298 K) and experimental temperature T, respectively, k is the Boltzmann constant (8.62×10^{-5} eV), and c is a constant. The Ea value falls in the value range of 0.06 ~ 0.57 eV that reported in the literatures.[36-38] The results above show that the ZGEN sample has a good thermal stability under the excitation of 282-nm UV light.

4. Conclusion

In this work, we have successfully synthesized $ZnGa_2O_4:Ni^{2+},Eu^{3+}$ persistent luminescent phosphors *via* a traditional high temperature solid-state reaction, which feature a broad emission band located in the second near-infrared (NIR-II) window. The samples were characterized by XRD, TEM, PLE/PL spectroscopy, lifetime, persistent luminescence decay and temperature-dependent PL spectra analysis. Ni^{2+} and Eu^{3+} are likely to occupy Ga^{3+} site in $ZnGa_2O_4$, forming a six-coordinated octahedron. The samples can not only be excited by ultraviolet (UV) light but also by orange-red light, in which, the emission spectrum of $ZnGa_2O_4:0.02Eu^{3+}$ and the excitation spectrum of $ZnGa_2O_4:0.005Ni^{2+}$ have a large overlap. Besides, under 282 nm UV excitation, an energy transfer from Eu^{3+} to Ni^{2+} ions could be observed which improves the NIR emission intensity. After removing the light source, the sample outputs both red and NIR afterglow, which can last more than 500 s. With the increase of Ni^{2+} ion concentration, however, the red afterglow monitored at 616 nm decreases significantly but the NIR afterglow increases, mainly due to the energy transfer. The ZGEN sample has a good thermal stability. The prepared persistent phosphors are the potential materials for bio-imaging application in NIR-II window, due to their charming emissions and afterglows.

Acknowledgements

This work was supported in part by the Natural Science Foundation of Liaoning Province (Grant 2020–MS–081), and National Natural Science Foundation of China (Grant 51302032, U21A2045, 52172112).

References

[1] Pei P, Chen Y, Sun C, Fan Y, Yang Y, et al. X-ray-activated persistent luminescence nanomaterials for NIR-II imaging. Nat Nanotechnol. 2021;16:1011-1018.

[2] Mao M, An M, Zhang X, Chu P. In vitro and in vivo antibacterial activity of graphene oxidemodified porous TiO_2 coatings under 808-nm light irradiation. Rare Met. 2022;41:540-545.

[3] Kamimura S, Xu C-N, Yamada H, Terasaki N, Fujihala M. Long-persistent luminescence in the near-infrared from Nd^{3+}-doped Sr_2SnO_4 for in vivo optical imaging. Jpn J Appl Phys. 2014;53:092403.

[4] Li C, Wang Q. Challenges and opportunities for intravital near-infrared fluorescence imaging technology in the second transparency window. ACS Nano. 2018;12:9654-9659.

[5] Liu F, Liang Y, Chen Y, Pan Z. Divalent nickel-activated gallate-based persistent phosphors in the short-wave infrared. Adv Optical Mater. 2016;4:562-566.

[6] Gao Y, Wang B, Liu L, Shinozaki K. Near-infrared engineering for broad-band wavelength-tunable in biological window of NIR-Ⅱ and -Ⅲ: A solid solution phosphor of $Sr_{1-x}Ca_xTiO_3$:Ni^{2+}. J Lumin. 2021;238:118235.

[7] Hölsä J. Persistent luminescence beats the afterglow: 400 years of persistent luminescence. Electrochem Soc Interface. 2009;18:42-45.

[8] Matsuzawa T, Aoki Y, Takeuchi N, Murayama Y. A new long phosphorescent phosphor with high brightness, $SrAl_2O_4$:Eu^{2+},Dy^{3+}. J Electrochem Soc. 1996;143:2670-2673.

[9] Pan Z, Lu Y-Y, Liu F. Sunlight-activated long-persistent luminescence in the near-infrared from Cr^{3+}-doped zinc gallogermanates. Nat Mater. 2011;11:58-63.

[10] Zhang Y, Li X, Lai Z, Zhang R, Lewis E, et al. Largest enhancement of broadband near-infrared emission of Ni^{2+} in transparent nanoglass ceramics: using Nd^{3+} as a sensitizer and Yb^{3+} as an energy-transfer bridge. J Phys Chem C. 2019;123:10021-10027.

[11] Yu G, Wang W, Jiang C. Linear tunable NIR emission via selective doping of Ni^{2+} ion into ZnX_2O_4 (X=Al, Ga, Cr) spinel matrix. Ceram Int. 2021;47:17678-17683.

[12] Yu G, Wang W, Jiang C. A facile approach towards fabrication and ultrabroad band emission properties of nickel ion-doped $ZnAl_2O_4$ transparent ceramics. Ceram Int.2020;46:10320-10324.

[13] Y S, Zhang Y, He H, Qiu J, Dong G. Simultaneous broadband near-infrared emission and magnetic properties of single phase Ni^{2+}-doped β-Ga_2O_3 nanocrystals *via* mediated phase-controlled synthesis. J Mater Chem C. 2015;3:2886-2896.

[14] Yuan L, Jin Y, Zhu C, Mou Z, Xie G, Hu Y. Ni^{2+}-doped yttrium aluminum gallium garnet phosphors: Bandgap engineering for broad-band wavelength-tunable shortwave-infrared long-persistent luminescence and photochromism. ACS Sustainable Chem. Eng. 2020;8:6543-6550.

[15] Yang H, Xiahou J, Zhu Q, Li J-G. Considerable improved near-infrared luminescence in ionic-free doped $ZnAl_2O_4$ by oxygen defects engineering. J Lumin. 2023;253:119455.

[16] Zhu Q, Xiahou J, Li X, Sun X, Li J-G. Defect cluster engineering in $ZnGa_{2-x}(Mg/Ge)_xO_4$:Cr^{3+} nanoparticles for remarkably improved NIR persistent luminescence. J Am Ceram Soc. 2021;104:4594-4605.

[17] Xiahou J, Zhu Q, Zhu L, Huang S, Zhang T, Sun X, Li J-G. Lattice-site engineering

in $ZnGa_2O_4$:Cr^{3+} through Li^+ doping for dynamic luminescence and advanced optical anti-counterfeiting. J Mater Chem C. 2022;10:7935-7948.

[18] Yang L, Zhao Y, Yin R, Li F. Synthesis of Ni^{2+}-doped $ZnAl_2O_4$/ZnO composite phosphor film with largely enhanced polychromatic emission via a single-source precursor. J Am Ceram Soc. 2014;97:1123-1130.

[19] Zhou Z, Zhong Y, Xia M, Zhou N, Lei B, Wang J, Wu F. Tunable dual emission of $Ca_3Al_4ZnO_{10}$:Bi^{3+},Mn^{4+} *via* energy transfer for indoor plant growth lighting. J Mater Chem C. 2018;6:8914-8922.

[20] Si T, Zhu Q, Zhang T, Sun X, Li J-G. Co-doping Mn^{2+}/Cr^{3+} in $ZnGa_2O_4$ to fabricate chameleon-like phosphors for multi-mode dynamic anti-counterfeiting. Chem Eng J. 2021;426:131744.

[21] Huang S, Xiahou J, Zhu Q, Takei T, Kim BN, Li J-G. Malate-aided selective crystallization and luminescence comparison of tetragonal and monoclinic $LaVO_4$:Eu nanocrystals. Dalton Trans. 2021;50:10147-10158.

[22] Chikoidze E, Sartel C, Madaci I, Mohamed H, et al. p-Type Ultrawide-Band-Gap Spinel $ZnGa_2O_4$:New Perspectives for Energy Electronics. Cryst Growth Des. 2020;20:2535-2546.

[23] Kück S. Laser-related spectroscopy of ion-doped crystals for tunable solid-state lasers. Appl Phys B. 2014;72:515-562.

[24] Li F, Li J-G, Zhu Q. EDTA-promoted aliovalent Eu^{3+} doping of $Sr_5(PO_4)_3F$ apatite, growth behavior and luminescence. Opt Mater. 2020;101:109765.

[25] Li F, Jin M, Li Z, Wang X, Zhu Q, Li J-G. Vertically aligned $Gd_2O_2SO_4$:Ln and Gd_2O_2S:Ln luminescent films with super-hydrophobicity via a novel precursor route (Ln = Pr, Eu, Tb). Appl Surf Sci. 2023;609:155323.

[26] Yao J, Zhu Q, Li J-G. Garnet transparent ceramic film of $Y_3Al_5O_{12}$:Eu^{3+} fabricated through an interface reaction of layered rare-earth hydroxide nanosheets on amorphous alumina. Appl Surf Sci. 2022;579:152226.

[27] Jin M, Li F, Xiahou J, Zhu L, Zhu Q, Li J-G. A new persistent luminescence phosphor of $ZnGa_2O_4$:Ni^{2+} for the second near-infrared transparency window. J Alloys Compd. 2023;931:167491.

[28] Xiahou J, Zhu Q, Li F, Jin M, Zhu L, Huang S, Zhang T, Sun X, Li J-G. Regulating the trap distribution of $ZnGa_2O_4:Cr^{3+}$ by Li^+/Ga^{3+} doping for upconversion-like trap energy transfer NIR persistent luminescence. Inorg Chem Front. 2023;10:2174-2188.

[29] Nie J, Li Y, Liu S, Chen Q, Xu Q, Qiu J. Tunable long persistent luminescence in the second near-infrared window via crystal field control. Sci Rep. 2017;7:12392.

[30] Paulose PI, Jose G, Thomas V, Unnikrishnan NV, Warrier M. Sensitized fluorescence of Ce^{3+}/Mn^{2+} system in phosphate glass. J Phys Chem Solids. 2003;64:841-846.

[31] Blasse G. Energy transfer in oxidic phosphors. Phys Lett A. 1968;28:444-445.

[32] Li F, Zhang M, Hou G, Shen Y, Liu Z, Li H. Sol-gel preparation and phosphorescence property of Mn^{2+}-doped zinc borosilicate glass thin films. Rare Met. 2011;30:298-303.

[33] Jiao H, Liao F, Tian S, Jing X. Luminescent Properties of Eu^{3+} and Tb^{3+} Activated $Zn_3Ta_2O_8$. J Electrochem Soc. 2003;150:220-224.

[34] Zhou Y, Zhuang W, Hu Y, Liu R, Xu H, Chen M, et al. Cyan-green phosphor $(Lu_2M)(Al_4Si)O_{12}:Ce^{3+}$ for high-quality LED Lamp: tunable photoluminescence properties and enhanced thermal stability. Inorg Chem. 2019;58:1492-1500.

[35] Guo Y, Zhou S, Sun X, Lao X, Yuan H. $BaAl_{12}O_{19}:Eu^{2+}$ phosphors: molten salt flux synthesis and blue emission with high color purity and excellently thermal stability. J Lumin. 2019;211:271-275.

[36] Mao Q, Shen B, Yang T, Zhong J, Wu G. A double perovskite-based red-emitting phosphor with robust thermal stability for warm WLEDs. Ceram Int. 2020;46:19328-19334.

[37] Zhao J, Guo C, Li T, Su X, Zhang N, Chen J. Synthesis, electronic structure and photoluminescence properties of $Ba_2BiV_3O_{11}:Eu^{3+}$ red phosphor. Dyes Pigm. 2016;132:159-166.

[38] Bi W, Meng Q, Sun W. Luminescent properties and energy transfer mechanism of $NaGd(MoO_4)_2:Sm^{3+},Eu^{3+}$ phosphors. Ceram Int. 2016;42:14086-14093.

Incorporation of Eu^{3+} in $ZnGa_2O_4$:Ni^{2+} for improved NIR persistent luminescence located in second transparency window

Minghui Jin[1], Tao Zhang[2], Ji-Guang Li[3], Qi Zhu[1*]

[1]*Key Laboratory for Anisotropy and Texture of Materials (Ministry of Education), School of Materials Science and Engineering, Northeastern University, Shenyang, Liaoning 110819, PR China*

[2]*Shenyang National Laboratory for Materials Science, Northeastern University, 3-11 Wenhua Road, Shenyang 110819, China*

[3]*Research Center for Functional Materials, National Institute for Materials Science, Namiki 1-1, Tsukuba, Ibaraki 305-0044, Japan*

*Corresponding author

Dr. Qi Zhu

Tel: +86-24-8367-2700

E-mail: zhuq@smm.neu.edu.cn

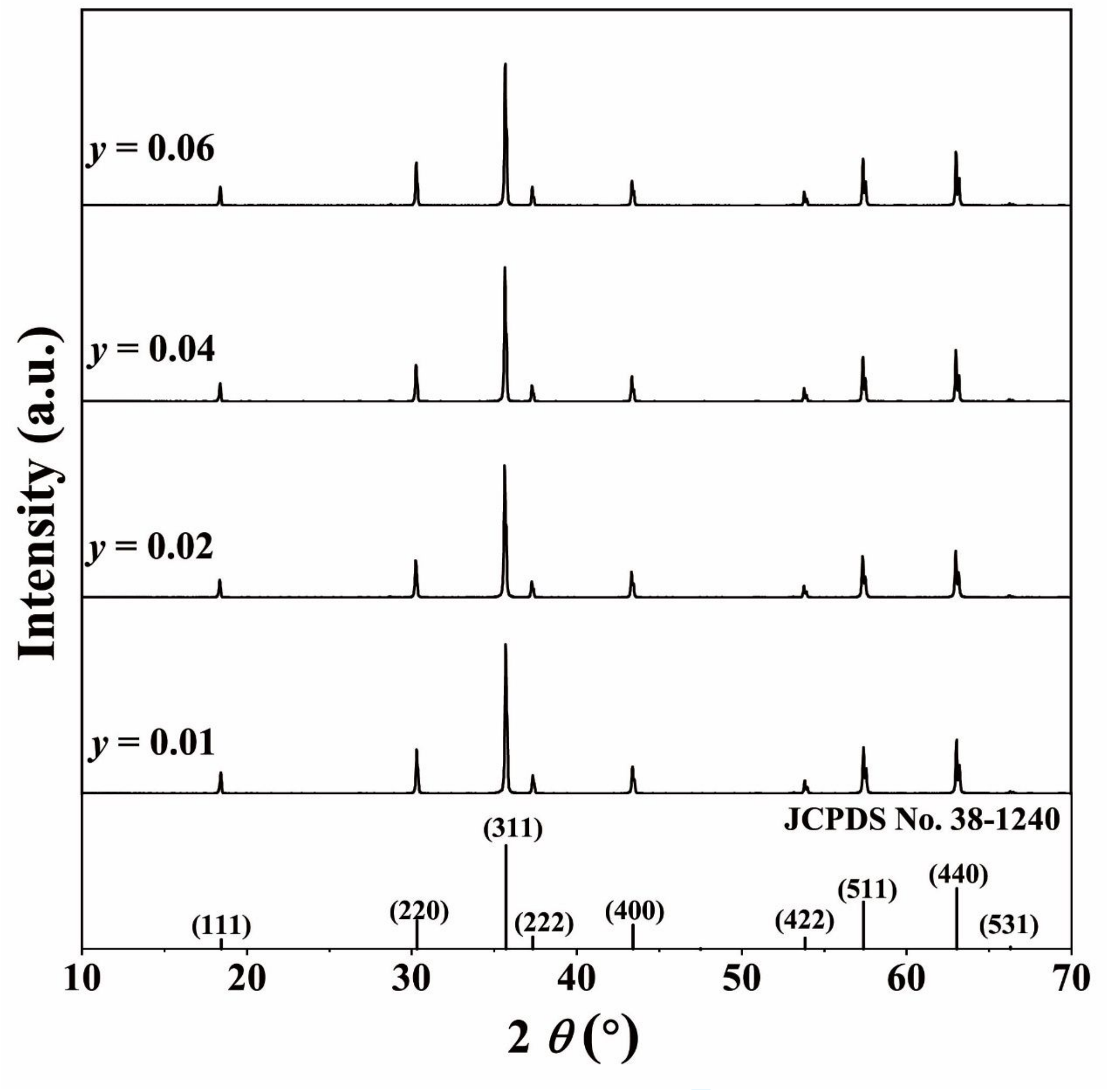

Fig. S1 XRD spectra of $ZnGa_2O_4$:$y$$Eu^{3+}$ samples

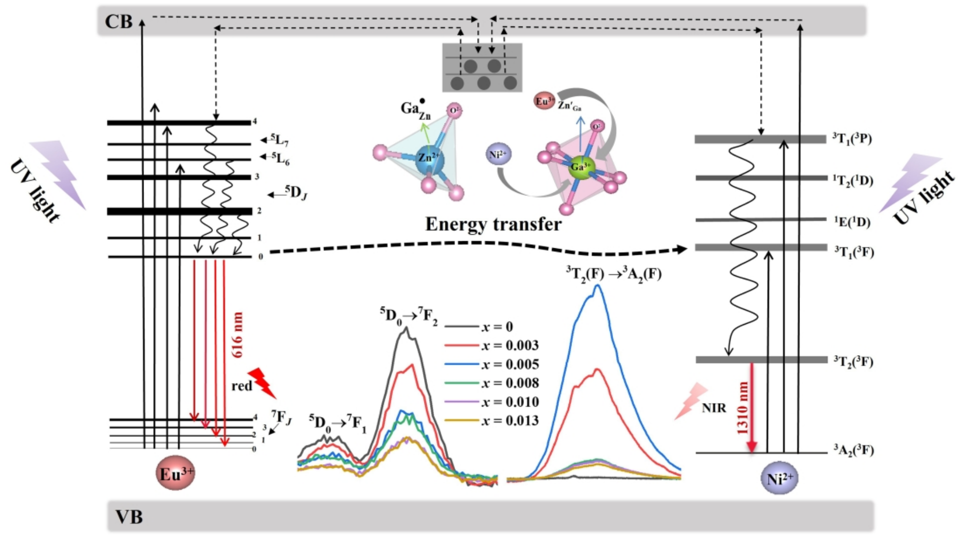

314x222mm (300 x 300 DPI)